Journal of Power Sources 214 (2012) 244–250

Contents lists available at SciVerse ScienceDirect

Journal of Power Sources

journal homepage: www.elsevier.com/locate/jpowsour

TiO_2 films with rich bulk oxygen vacancies prepared by electrospinning for dye-sensitized solar cells

Xiaodong Li [a], Caitian Gao [a], Jiangtao Wang [a], Bingan Lu [a,b], Wanjun Chen [a], Jie Song [a], Shanshan Zhang [a], Zhenxing Zhang [a], Xiaojun Pan [a], Erqing Xie [a,*]

[a] Key Laboratory for Magnetism and Magnetic Materials of the Ministry of Education, Lanzhou University, Lanzhou 730000, Gansu, PR China
[b] Key Laboratory for Micro-Nano Optoelectronic Devices of Ministry of Education, State Key Laboratory for Chemo/Biosensing and Chemometrics, Hunan University, Hunan, PR China

HIGHLIGHTS

- Transparent TiO_2 films were prepared by electrospinning.
- TiO_2 films with rich bulk oxygen vacancies induce large V_{oc} and FF in DSCs.
- We first used an unsensitized cell to investigate the trap-to-trap electron transport.
- The results from PL measurement show useful information.

ARTICLE INFO

Article history:
Received 8 January 2012
Received in revised form
6 April 2012
Accepted 8 April 2012
Available online 4 May 2012

Keywords:
Dye-sensitized solar cells
Open-circuit voltage
Photoluminescence
Bulk/surface oxygen vacancy
Electrospinning

ABSTRACT

Highly transparent nanocrystalline TiO_2 films have been fabricated by electrospinning (ES) technique based on a transmutation process from as-spun nanofibers with an appropriate amount of triethanolamine (TEOA) added to the precursor. A possible evolution mechanism of the transparent nanocrystalline TiO_2 films is proposed. It is found that the films prepared via transmutation from electrospun nanofibers possess rich bulk oxygen vacancies (BOVs, PL band at 621–640 nm) by using photoluminescence (PL) spectroscopy. Contrastively, the dominant peak in PL spectrum of the spin-coated film is the emission from surface oxygen vacancies (SOVs, PL band at 537–555 nm). The electrospun TiO_2 films with rich BOVs induce large open-circuit voltage (V_{oc}) and fill factor (*FF*) improvements in dye-sensitized solar cells (DSCs), and thus a large improvement of energy conversion efficiency (η). In addition, these performance advantages are maintained for a double-layer cell with a doctor-bladed ~7 μm top layer (P25 nanometer TiO_2, Degussa) and an electrospun ~3 μm bottom layer. The double-layer cell yields a high η of 6.01%, which has increased by 14% as compared with that obtained from a 10 μm thick P25 film.

1. Introduction

Dye-sensitized solar cells (DSCs) have attracted extensive interest in the past decade due to the prospects of low-cost, environment-friendly, high-performance and of new applications such as transparent solar cells and flexible solar cells [1–4]. Nanostructured metal oxides are one of the key factors in determining the photovoltaic-characteristics of DSCs, because the nanostructured networks will act as a scaffold for the dyes and a transfer media for photogenerated electrons to the transparent conductive oxide layer. Therefore, the properties of the metal oxides, such as the defects in the materials, must greatly influence the photovoltaic-characteristics of DSCs.

In DSCs, the photogenerated electrons would transfer directly from the conduction band or the surface traps of TiO_2 nanoparticles [5–7] to acceptors in electrolyte. Thus the traps located at the TiO_2 surface would lower the electron lifetime in DSCs and resulting in poor cell performance [8]. For this reason, various methods have been developed to improve the cell performance by minimizing the possible recombination pathways occurring at the TiO2|dye|electrolyte interface [9–11]. However, the electron traps in the bulk may behave differently. As the trap sites are filled, the potential difference between the highest filled traps and the conduction band decreases. This may increase excitation possibility of the trapped electrons from the traps to the conduction band. Furthermore, the bulk traps trap and release electrons only

* Corresponding author.
E-mail addresses: lixd04@163.com (X. Li), xieeq@lzu.edu.cn (E. Xie).

0378-7753/$ – see front matter © 2012 Elsevier B.V. All rights reserved.
doi:10.1016/j.jpowsour.2012.04.042

with the conduction band [6], namely the bulk traps are unable to transfer electrons to the acceptor species in electrolyte solution. Nelson et al. [7] demonstrated that multiple trapping with a broad energetic distribution of electron traps is responsible for the slow recombination kinetics in DSCs. Thus, using TiO_2 films with rich bulk electron traps may be a practical strategy to achieve the high photovoltaic performance, which is of great importance but has not been done.

As a simple and cost-effective way to prepare semiconductor oxides with 1D nanostructure, electrospinning technique has attracted extensive interest in various areas, including dye-sensitized solar cells [12], gas sensor [13], photo-catalysis [14], lithium-ion batteries [15], and transparent conductive films [16]. Compared with other methods, electrospinning possesses many advantages, such as large-area preparation, on both conductive and insulating substrates, and cost-effective. It is reported that different nanostructures, for example, nanofibers [17], nanotubes [18] and nanobelts [19] have been fabricated by electrospinning technique. Here, we report the preparation of highly transparent nanocrystalline TiO_2 films by electrospinning. The resultant films possess rich bulk oxygen vacancies and can induce large open-circuit voltage (V_{oc}) and fill factor (FF) improvements in DSCs.

2. Experimental details

2.1. Preparation of the transparent nanocrystalline TiO_2 films

To prepare the precursor solutions, 0.5 g tetrabutyl titanate (≥98%) was dissolved in a mixture of 1 ml acetic acid and 1 ml ethanol. The obtained solution was stirred for 10 min to form a sol. Then, a solution containing 0.19 g poly (vinyl pyrrolidone) (PVP, Sigma Aldrich, Mw ≈ 1,300,000), 1.5 ml ethanol and 0.5 ml N,N-Dimethylformamide (DMF) were mixed with the above sol. After stirring the obtained solution for 20 min, tri-ethanolamine (TEOA) was added. Finally, the precursor was obtained after stirring the solution for 30 min. The applied voltage and the distance between the nozzle and the collector were fixed at 6.5 kV and 10 cm, respectively. To achieve the transmutation of the electrospun nanofibers, the humidity level was controlled at 50–55%.

2.2. Assembling of DSCs

All TiO_2 electrodes were sintered at 500 °C for 2 h. For the post-treatment, the TiO_2 films were dipped into a 100 mM $TiCl_4$ aqueous solution for 20 min at 70 °C, then sintered again at 500 °C for 30 min. At 80 °C in the cooling, the sintered TiO_2 electrodes were immersed into a 0.3 mM solution of N-719 dye in a mixture of tert-butyl alcohol and acetonitrile (volume ratio of 1:1) and kept in the dark at room temperature for 12 h to complete the adsorption of the dye. The platinized counter electrode was fabricated by spin-coating a 6.0 mM isopropanol solution of $H_2PtCl_6{\bullet}6H_2O$, then annealing at 400 °C for 20 min. The electrolyte was a solution of 0.1 M LiI, 0.6 M 1,2-dimethyl-3-propylimidazorium iodide, 0.06 M I_2 and 0.5 M 4-tert-butylpyridine in acetonitrile. The preparation of a P25 based paste for reference is described in our previous work [20]. The cell area was fixed at 0.45 cm^2.

2.3. Characterization

Morphologies and optical properties were studied by field emission scanning electron microscopy (FESEM, Hitachi, S-4800) and UV–VIS spectrophotometer (TU-1901), respectively. X-ray diffraction (XRD) (Philips X'pert Pro MPD (Cu Kα ray)) was used to characterize the crystallographic property. PL measurements were carried out on a Raman spectroscopy (JY-HR800) with a 325 nm line of 50 mW diode-pumped solid state laser at room temperature. AC impedance spectroscopy was performed on an electrochemical system (RST-5200, Zhengzhou Shiruisi Instrument Technology Co., Ltd, China) with frequency range from 0.1 to 10^5 Hz and the oscillation amplitude of 10 mV. Thicknesses of the TiO_2 films were obtained by using a surface profile measurement system (Veeco, Dektak8).

3. Results and discussion

3.1. The effect of TEOA on TiO_2 films

Without TEOA in the precursor, a nanofiber mat (Fig. 1(a)) was formed, which is a common result achieved by many other groups

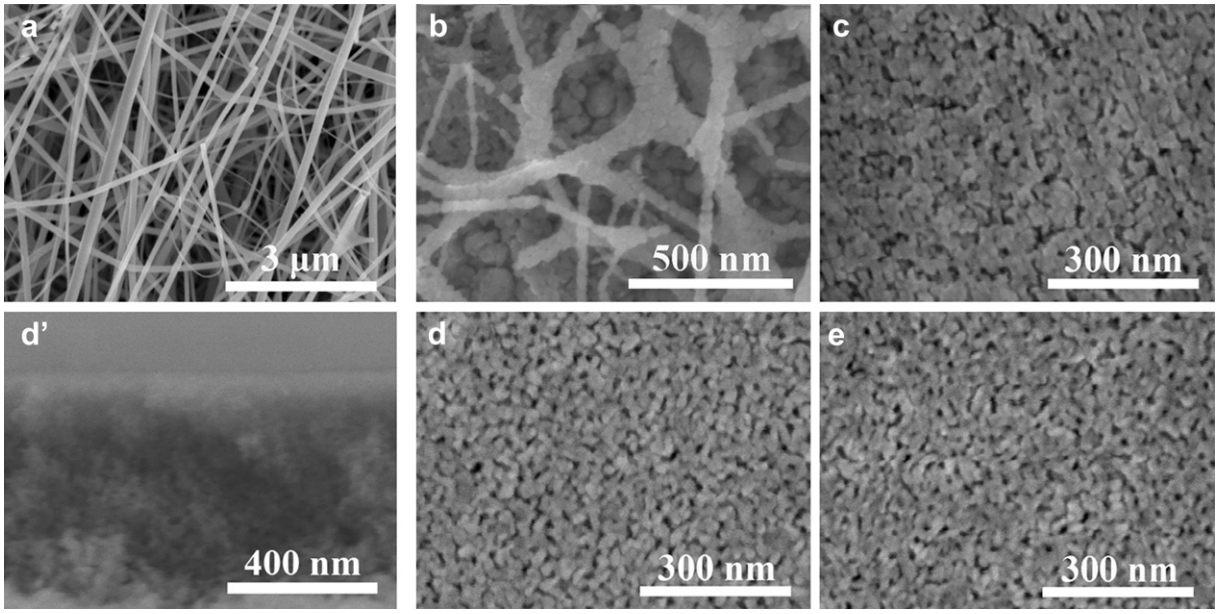

Fig. 1. FESEM images of the electrospun samples with precursor solutions consisting of 0 (a), 3.8 (b), 5.0 (c), 6.3 (d) and 8.5 wt.% (e) TEOA. Cross-sectional SEM image of the film with 6.3 wt.% TEOA (d'). All the samples were annealed at 500 °C for 2 h.

[21]. With a small amount of TEOA added, such as 3.8 wt.%, a nanofibers-covered nanocrystalline film is obtained (Fig. 1(b)). This film is consisted of hierarchical aggregates with average diameter ranging from 65.3 nm to 135.5 nm, and the size of the primary nanoparticles in the aggregates is between 14.9 nm and 40.1 nm. As the proportion of TEOA increased, the nanofibers disappeared gradually and films were formed with an increasing uniformity of the particle sizes (Fig. 1(c)–(e)). Moreover, when the proportion of TEOA was increased from 3.8 wt.% to 8.5 wt.%, the average particle sizes of the films decrease from 32.0 nm to 18.5 nm (Fig. 2). Cross-sectional SEM image of the films with 6.3 wt.% TEOA shown in Fig. 1(d') reveals that the film consists of uniform nanoparticles with an average size of ~23 nm, which is consistent with the surface morphology shown in Fig. 1(d). In addition, the films exhibit high transparency and large area uniformity as shown in Fig. S1.

3.2. Formation mechanism of the transparent nanocrystalline TiO_2 films

A possible evolution mechanism of the transparent nanocrystalline TiO_2 films is shown in Fig. 3. With TEOA in the precursor, the nanofibers cannot keep their shape and may transmute from nanofiber mat to a continuous gel layer due to the intrinsic hygroscopic and viscous properties of TEOA. Because it is viscous, the TEOA is hardly to evaporate and make the nanofibers deform easily. Because it is hygroscopic, TEOA can absorb the moisture in the air which will redound to the nanofibers deformation process. Here, a high humidity of 50–55% is required. It was reported that TEOA acts as an inhibitor of the coagulation of the growing hydroxide particles [22]. With a small amount of TEOA was added, such as 3.8 wt.%, the transmutation process was not complete and a loose gel layer may form. During the process, coagulation of the growing hydroxide particles happened due to the high humidity and low content of TEOA, resulting in TiO_2 particles with larger size. While with a large amount of TEOA was added, such as 8.5 wt.%, the transmutation process was complete, resulting in a compact gel layer. Because of the high concentration of TEOA, coagulation of the growing hydroxide particles is hindered, leading to TiO_2 particles with smaller particle sizes and better uniformity.

To assess the validity of the above mechanism, samples were fabricated by spin-coating by using the same precursors as that in

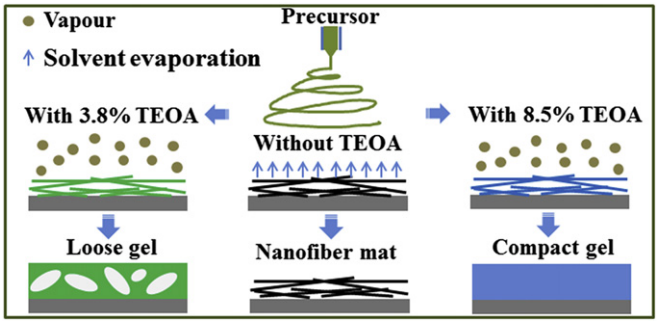

Fig. 3. Schematic diagram showing the effect of TEOA on the formation of the transparent nanocrystalline TiO_2 films.

electrospinning. As shown in Fig. 2, the particle sizes of the spin-coated samples stay the same which was in sharp contrast to that of electrospinning samples. This is because the gel layer formed on the substrate by spin-coating method is compact and is irrelevant to the proportion of TEOA. While for electrospinning, the transmutation happens on the substrate under the combined action of TEOA and humidity, which is dependent on the proportion of TEOA.

3.3. Structural characterization

Fig. 4 shows the XRD spectra of TiO_2 nanocrystalline films prepared by electrospinning and spin-coating using the precursor with 8.5 wt.% TEOA. The films were annealed in air at 500 °C for 2 h. Both samples show a typical anatase phase. PL measurement is a powerful technique to investigate the electronic structure and energy levels in the band-gap of semiconductor materials, which could influence the charge transport and recombination property in DSCs. Herein, we investigated the room-temperature PL spectra of the samples fabricated with various TEOA concentrations by electrospinning (Fig. 5(a)–(c)). For comparison, PL spectrum of the sample prepared by spin-coating with 8.5 wt.% TEOA (SC-8.5) is also shown in Fig. 5(d). It is necessary to indicate that the particle size of the film prepared by spin-coating was controlled to be ~17.8 nm by changing spin-coating parameters (Fig. S2), which is comparable to the particle size of the film by electrospinning with 8.5 wt.% TEOA (ES-8.5, Fig. 2). As shown in Fig. 5(a)–(d), all the PL bands can be

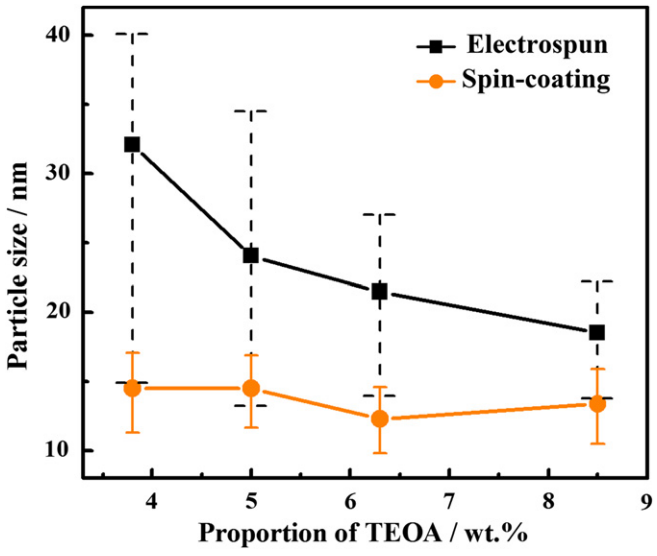

Fig. 2. Particle sizes as function of the proportion of TEOA.

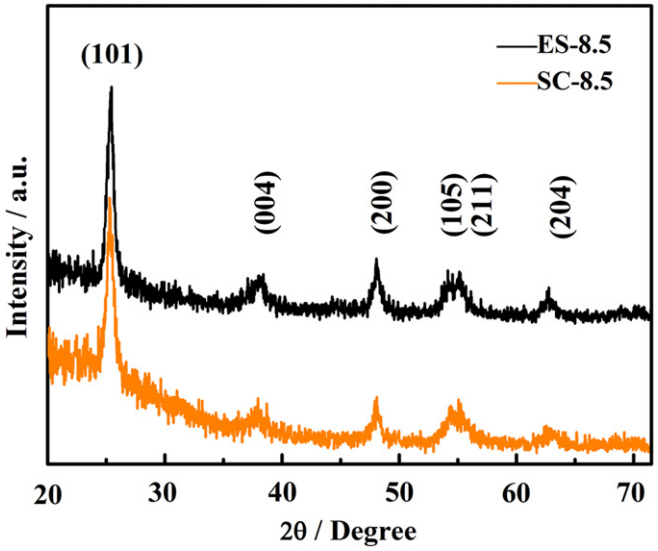

Fig. 4. XRD spectra of TiO_2 nanocrystalline films prepared by electrospinning and spin-coating using the precursors with 8.5 wt.% TEOA.

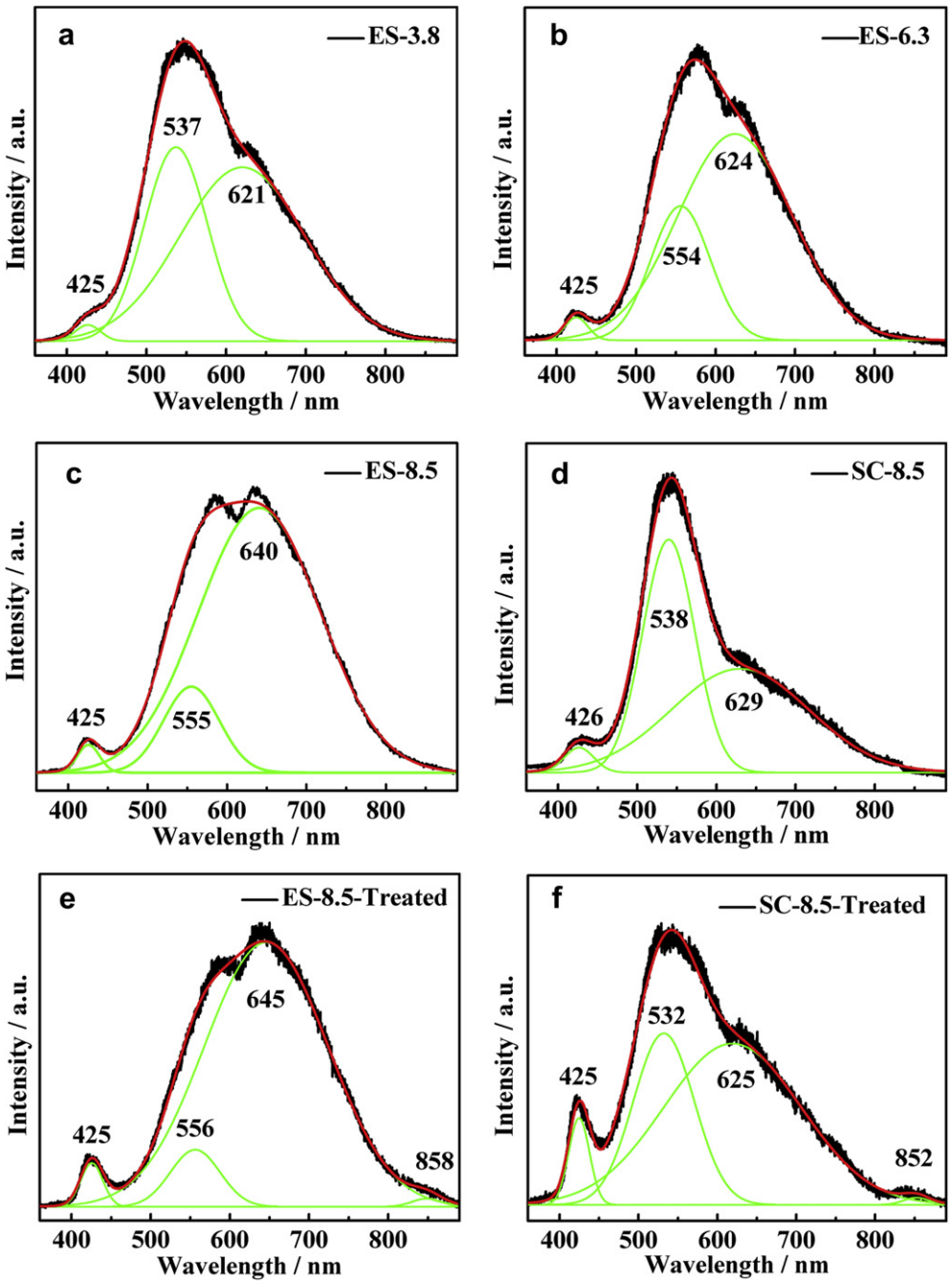

Fig. 5. PL spectra of nanocrystalline TiO_2 films prepared by electrospinning with different proportions of TEOA: 3.8 (a), 6.3 (b) and 8.5 wt.% (c), and by spin-coating with 8.5 wt.% TEOA (d). PL spectra of the films prepared by electrospinning (e) and spin-coating (f) with 8.5 wt.% TEOA after treatment by $TiCl_4$ aqueous solution.

fitted into three Gaussian peaks with wavelengths of 425–426 nm, 537–555 nm and 621–640 nm. As the proportion of TEOA increases, the intensity of the peaks at 621–640 nm increases and becomes dominant when the proportion of TEOA reaches 8.5 wt.%, which is in sharp contrast to that of the samples prepared by spin-coating method (Fig. 5(d)). To achieve successful transmutation of the electrospun nanofibers hygroscopic TEOA was added to the precursor and a high humidity level of 50–55% was kept. Thus, the significant difference in PL measurement between the two samples may result from the quick hydrolyze of tetrabutyl titanate during electrospinning.

Generally, PL spectra of anatase TiO_2 materials are interpreted as the emission from three physical origins: self-trapped excitons [23,24], oxygen vacancies (OVs) [25,26] and surface states [27]. In anatase TiO_2 materials, lattice relaxation energy (E_{lr}) is larger than the energy reduction ($B = \nu|y|$) in the delocalization process by transferring from one site to a neighbor site [23]. Under this condition, the self-trapped excitons on the TiO_6 octahedra recombine with impurity-trapped excitons radiatively. As shown in Fig. 5(a)–(d), the 425 nm bands hold constant regardless of the proportion of TEOA and the preparation method. Moreover, the peak position of the 425 nm band is very close to that in Ref. [24] (425 nm) and Ref. [26] (412 nm). So the 425 nm band should be accordingly assigned to self-trapped excitons (STE) localized on TiO_6 octahedra. PL bands at the long wavelength side of anatase TiO_2 nanoparticles have been attributed to the OVs [24–26].

Shallow traps identified with OVs were established at 0.8 eV below the conduction band [26]. Forss and Schubnell [27] have attributed the band corresponding to shallow traps to surface states. In our case, the 537–555 nm (0.89–0.96 eV) bands in Fig. 5(a)–(d) are very close to that in Ref. [26] (0.80 eV) and Ref. [24] (0.82 eV). Therefore, we assign the PL bands at 537–555 nm to OV located at the surface of the TiO_2 nanoparticles (SOVs), which can be confirmed later. There are another energy levels resulting from OV in TiO_2 at about 1.18 eV (614 nm) [28] below conduction band. Accordingly, we assign the PL bands at 621–640 nm to emission from oxygen vacancies. Furthermore, these oxygen vacancies are in the bulk of TiO_2 nanoparticles.

To demonstrate the origin of the PL bands, a rutile TiO_2 passivation layer was formed on the surface of the nanoparticles by a 100 mM $TiCl_4$ aqueous solution treatment at 70 °C for 20 min. In rutile TiO_2 materials, $B > E_{lr}$, the excitons are stabilized in the Free State. In this case the PL spectrum of rutile TiO_2 materials is either resulted from free exciton emission at low-temperature, or infrared emission from its intrinsic properties [23,29,30]. As shown in Fig. 5(e) and (f), the PL band at 852–858 nm proved the existence of rutile TiO_2 coating. No peak from free exciton emission of rutile TiO_2 is observed. It is found that the intensity of 537–555 nm bands decreases sharply after surface passivation, while the intensity of 425 nm and 621–640 nm bands are almost unchanged after treatment. Therefore, the 537–555 nm and 621–640 nm bands originate from the defects located at surface and in bulk of nanoparticles, respectively. In addition, the two bands are dominant peaks of the corresponding samples. These provide convenience to investigate the effect of different defects on the photovoltaic properties of DSCs.

3.4. Influence on photovoltaic-characteristics of DSCs

J–V curves recorded from the cells with 3 μm thick ES-8.5 (ES-3 μm) and SC-8.5 (SC-3 μm) TiO_2 films as photoanodes are shown in Fig. 6(a). ES-3 μm film gives an average η value of 2.43% compared with only 2.14% for the SC-3 μm film. The key observation here is that an increase of BOVs in TiO_2 film induces large V_{oc} and *FF* improvements, from 0.797 V and 0.559 for SC-3 μm to 0.826 V and 0.663 for ES-3 μm, respectively. These performance advantages are maintained when a ~7 μm thick TiO_2 film was doctor-bladed on top of the ~3 μm thick electrospun TiO_2 film from a P25 based paste [20], and this film was designated ES-3 μm + P25, as shown in Fig. 6(b). As compared with a 10 μm thick P25 film, the V_{oc} and FF values for ES-3 μm + P25 increase by 46 mV and 10.8%, respectively. The cumulative increases of V_{oc} and FF give rise to an efficiency of 6.01%, which has increased by 14% as compared with that obtained from a 10 μm thick P25 film.

To investigate the improvement of V_{oc} and FF by using ES-8.5 film, charge recombination lifetime (τ_r) [31] was measured through electrochemical impedance spectroscopy (EIS) technique. The impedance at the interface of TiO_2/dye/electrolyte appeared in the middle frequency range. The bode phase plots (frequency vs. phase angle) of the EIS results for the above two films are shown in Fig. 6(c). The characteristic frequencies at the peaks (f_{max}) is related to charge recombination lifetime ($\tau_r = 1/2\pi f_{max}$) [32]. As shown in

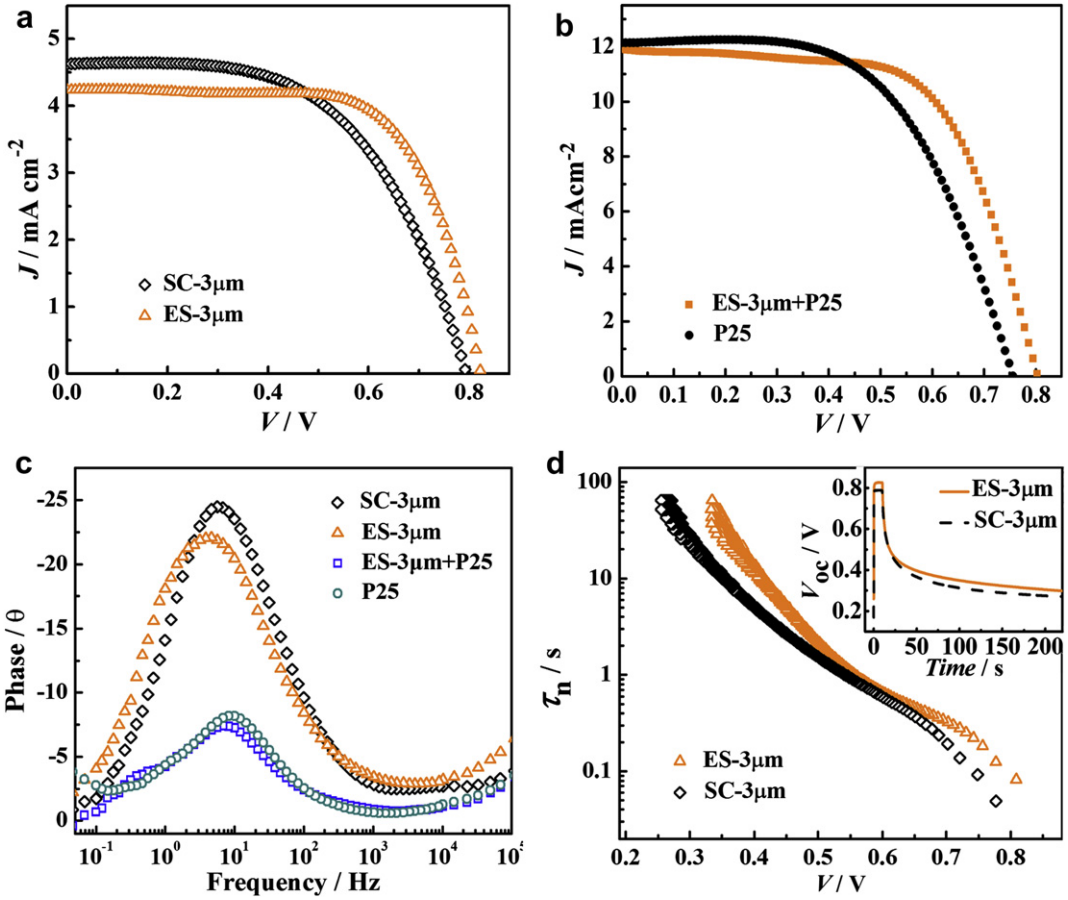

Fig. 6. *J–V* curves of DSCs with (a) ES-3 μm and SC-3 μm film and (b) ES-3 μm + P25 and P25 film as photoanodes. (c) Electrochemical properties of the bode plot measured by EIS analyzer for DSCs fabricated from ES-3 μm, SC-3 μm, ES-3 μm + P25 and P25 cells. (d) The electron lifetime for ES-3 μm and SC-3 μm cells as a function of V_{oc} derived from the open-circuit voltage-decay (OCVD) curve. The corresponding OCVD curves of ES-3 μm and SC-3 μm cells are shown in inset of (d). All the cell areas are 0.45 cm^2.

Fig. 6(c) and the corresponding parameters in Table 1, the τ_r of ES-8.5 (32.2 ms) film is larger than that of SC-8.5 (24.27 ms) film, revealing the increase of the electron lifetime by using TiO_2 film with rich BOVs. This advantage of τ_r is maintained when a ~7 μm thick P25 film was doctor-bladed on top of the ~3 μm thick ES-8.5 film. To a certain extent, as electron lifetime increases, recombination current decreases, resulting in an increase of V_{oc} [8]. FF is usually governed by the series resistance (R_s) which can be measured by EIS [33]. However, the R_s values of ES-8.5 and ES-3 μm + P25 films are very similar to that of SC-8.5 and P25 films, respectively, indicating that the increase of FF for ES-8.5 film is not due to the decrease of R_s. Further work should be done to explain how BOVs contribute to FF.

The advantages of open-circuit voltage-decay (OCVD) technique over the frequency or steady-state-based methods are that it provides a continuous reading of the lifetime as a function of V_{oc} at high-voltage resolution. The lifetime can be derived from the open-circuit voltage-decay curve by Equation (1) [34]:

$$\tau_n = -\frac{k_B T}{e}\left(\frac{dV_{oc}}{dt}\right)^{-1} \quad (1)$$

Where, k_BT is the thermal energy, e is the elementary charge, and dV_{oc}/dt is the first-order time derivative of the V_{oc}. Fig. 6(d) shows lifetime values obtained from the OCVD curves using Equation (1). The shapes of the τ_n–V_{oc} curve for ES-8.5 and SC-8.5 shows a trap-assisted conduction mechanism, which are in accordance with that of nanoparticles [6]. The larger τ_n for ES-8.5 film compared with that of SC-8.5 may be resulted from the rich BOVs. In addition, the depression seen in the curve at around 0.55 V indicates the effect of SOVs, which could result in recombination of electrons with the electrolyte through tunneling [35]. Therefore, the small difference of the τ_n at around 0.55 V for ES-8.5 and SC-8.5 indicates that the two films possess a similar surface texture.

To gain further insight into the effects of the electron traps, we designed a novel cell that has the same structure as the conventional DSCs but without dye adsorption. Without dye molecules, the photovoltaic properties of the cells are just dependent on the inherent electronic structure of TiO_2. Thus, the effect of BOVs on the photovoltaic properties of DSCs can be enlarged. To find a direct evidence of the effect of BOVs on V_{oc}, we measured the spectral responses of J_{sc} and V_{oc} in the wavelength range from 370 nm to 900 nm for film ES-8.5 and SC-8.5. As shown in Fig. 7, three humps located at 390–450 nm, 450–590 nm and 600–760 nm can be observed for both ES-8.5 and SC-8.5, the locations of which match well with the three Gauss bands fitted from PL spectra. As can be seen from Fig. 7, the V_{oc} for ES-8.5 film is higher than that of SC-8.5 film across the whole wavelength range from 370 nm to 900 nm; whereas the J_{sc} is just the reverse. Notably, the peak values of V_{oc} at 600–760 nm are 0.198 V for SC-8.5 and 0.306 V for ES-8.5, the latter is much higher than the former, which is a direct evidence of the effect of BOVs on the V_{oc} of DSCs.

Based on the above experiments, we believe that the rich BOVs in ES-8.5 film are the source of the improved V_{oc} and FF. A schematic diagram was draw to illustrate the source of the photovoltaic effect related to STE, SOVs and BOVs, as shown in Fig. 8. Generally,

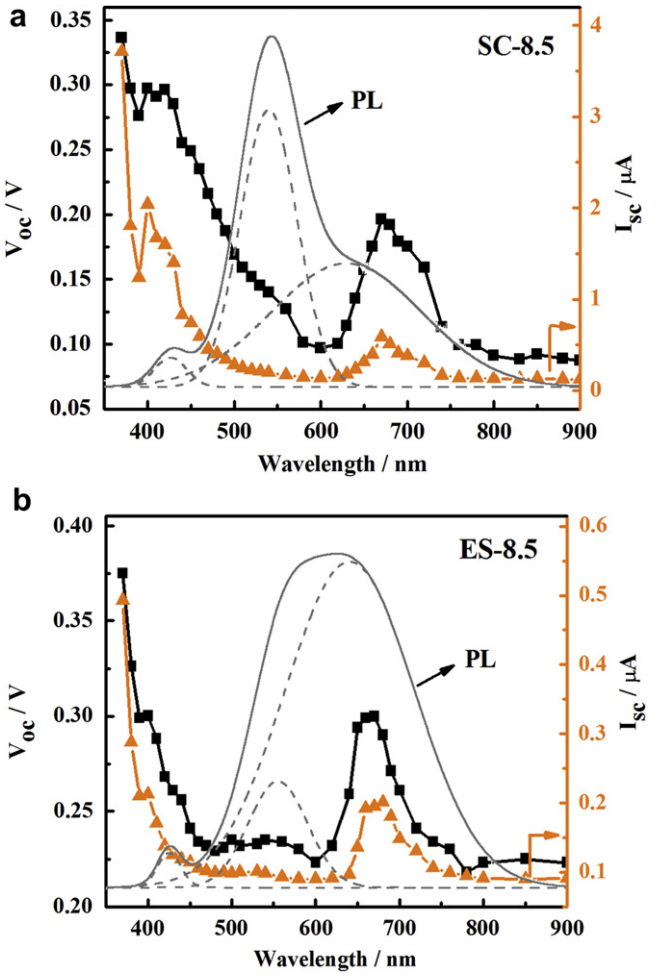

Fig. 7. The spectral responses of the cells with ES-8.5 and SC-8.5 film as photoanodes without dye adsorption. The homogeneous light intensity was fixed at 200 mW cm^{-2}.

the steady state DSC performance modeling is solely based on the conduction band electrons and neglects the influence of electron trapping [36]. However, in this work we have demonstrated that the trap-to-trap electron transport and direct recombination from the trap states are indeed happening in DSCs. The electron trapping, transport and recombination processes are shown in Fig. 8. The photons with energy lower than the band gap of TiO_2 promote electrons from the valence band (VB) to trap states in the band gap, followed by trap-to-trap electron transport process and direct recombination from the trap states process. It is necessary to point out that the maximum value of both V_{oc} and J_{sc} corresponding to BOVs is at wavelength of 670 nm, which possess a redshift of ~30 nm as compared with that of the PL bands from BOVs. This may be because that the traps with energy levels lower than reduction potential of the electrolyte offer an additional pathway to electron transport: the photons promote trapped electrons to trap states in the band gap and/or to CB, followed by trap-to-trap

Table 1
Summary of photovoltaic and electrochemical properties of the cells in Fig. 6. Each value was an average of three measurements.

Samples	J_{sc} [mA cm^{-2}]	V_{oc} [V]	*FF*	η [%]	R_s [Ω]	τ_r [ms]	Adsorbed dye [$\times 10^{-8}$ mol cm^{-2}]
ES-8.5	4.43 ± 0.10	0.826 ± 0.007	0.663 ± 0.017	2.43 ± 0.06	29.83 ± 1.15	32.2 ± 2.2	3.79
SC-8.5	4.81 ± 0.10	0.797 ± 0.006	0.559 ± 0.007	2.14 ± 0.08	29.16 ± 0.19	24.27 ± 2.67	3.85
ES-3 μm + P25	11.96 ± 0.09	0.800 ± 0.003	0.628 ± 0.003	6.01 ± 0.06	26.78 ± 0.58	19.50 ± 0.33	12.08
P25	12.24 ± 0.11	0.750 ± 0.006	0.567 ± 0.008	5.23 ± 0.04	26.57 ± 0.72	17.15 ± 0.13	11.85

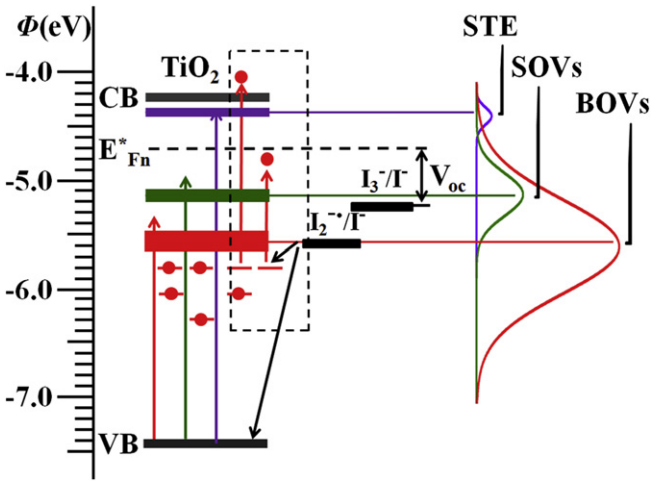

Fig. 8. Schematic illustration showing the source of the photovoltaic effect related to STE, SOVs and BOVs.

electron transport process and/or diffusion process, Fig. 8 (see in rectangle box).

4. Conclusions

In conclusion, with TEOA added to the precursor, transmutation from electrospun nanofibers to transparent nanocrystalline films can be achieved. The proportion of TEOA and the humidity level are two crucial factors in preparation of the transparent nanocrystalline TiO_2 films. It is found that the emissions from BOVs in electrospun films increase with the proportion of TEOA increasing, and become a dominant peak with 8.5 wt.% TEOA added to the precursor. Contrastively, the dominant peak in PL spectrum of the spin-coated film comes from the emission from SOVs. DSCs fabricated from ES-8.5 film show much higher V_{oc} and *FF* than that of SC-8.5. By using a double-layer cell with a doctor-bladed ~7 μm top layer and an electrospun ~3 μm bottom layer, the cumulative increases of V_{oc} and FF give rise to an efficiency of 6.01%, which has increased by 14% as compared with that obtained from a 10 μm thick P25 film. With the help of EIS measurement and OCVD, we conclude that the BOVs are responsible for the high V_{oc} and FF.

Acknowledgements

This work was financially supported by the National Natural Science Foundation of China (No. 61176058), the Fundamental Research Funds for the Central Universities (No. lzujbky-2011-149 and lzujbky-2012-34).

Appendix A. Supporting information

Supplementary material associated with this article can be found, in the online version, at doi:10.1016/j.jpowsour.2012.04.042

References

[1] B. O'Regan, M. Grätzel, Nature 353 (1991) 737.
[2] M. Grätzel, Nature 414 (2001) 338.
[3] M.G. Kang, N.-G. Park, Y.J. Park, K.S. Ryu, S.H. Chang, Sol. Energy Mater. Sol. Cells 75 (2003) 475–479.
[4] S. Yoon, S. Tak, J. Kim, Y. Jun, K. Kang, J. Park, Build. Environ. 46 (2011) 1899–1904.
[5] G. Schlichthörl, S.Y. Huang, J. Sprague, A.J. Frank, J. Phys. Chem. B 101 (1997) 8141–8155.
[6] J. Bisquert, A. Zaban, M. Greenshtein, I. Mora-Seró, J. Am. Chem. Soc. 126 (2004) 13550–13559.
[7] J. Nelson, S.A. Haque, D.R. Klug, J.R. Durrant, Phys. Rev. B 63 (2001) 205321.
[8] A. Usami, S. Seki, Y. Mita, H. Kobayashi, H. Miyashiro, N. Terada, Sol. Energy Mater. Sol. Cells 93 (2009) 840–842.
[9] V. Ganapathy, B. Karunagaran, S.W. Rhee, J. Power Sources 195 (2010) 5138–5143.
[10] B.A. Gregg, F. Pichot, S. Ferrere, C.L. Fields, J. Phys. Chem. B 105 (2001) 1422–1429.
[11] K. Park, Q. Zhang, B.B. Garcia, X. Zhou, Y.-H. Jeong, G. Cao, Adv. Mater. 22 (2010) 2329–2332.
[12] W. Zhang, R. Zhu, X. Liu, B. Liu, S. Ramakrishna, Appl. Phys. Lett. 95 (2009) 043304–043303.
[13] B. Ding, M. Wang, J. Yu, G. Sun, Sensors 9 (2009) 1609–1624.
[14] D. Lin, H. Wu, R. Zhang, W. Pan, Chem. Mater. 21 (2009) 3479–3484.
[15] L. Ji, Y. Yao, O. Toprakci, Z. Lin, Y. Liang, Q. Shi, A.J. Medford, C.R. Millns, X. Zhang, J. Power Sources 195 (2010) 2050–2056.
[16] H. Wu, L. Hu, M.W. Rowell, D. Kong, J.J. Cha, J.R. McDonough, J. Zhu, Y. Yang, M.D. McGehee, Y. Cui, Nano Lett. 10 (2010) 4242–4248.
[17] Y.X.D. Li, Adv. Mater. 16 (2004) 1151–1170.
[18] W. Wang, J. Zhou, S. Zhang, J. Song, H. Duan, M. Zhou, C. Gong, Z. Bao, B. Lu, X. Li, W. Lan, E. Xie, J. Mater. Chem. 20 (2010) 9068–9072.
[19] Y. Su, B. Lu, Y. Xie, Z. Ma, L. Liu, H. Zhao, J. Zhang, H. Duan, H. Zhang, J. Li, Y. Xiong, E. Xie, Nanotechnology 22 (2011) 285609.
[20] X. Li, Y. Zhang, Z. Zhang, J. Zhou, J. Song, B. Lu, E. Xie, W. Lan, J. Power Sources 196 (2011) 1639.
[21] R. Zhu, C.-Y. Jiang, X.-Z. Liu, B. Liu, A. Kumar, S. Ramakrishna, Appl. Phys. Lett. 93 (2008) 013102–013103.
[22] T. Sugimoto, T. Kojima, J. Phys. Chem. C 112 (2008) 18760–18771.
[23] H. Tang, H. Berger, P.E. Schmid, F. Lévy, G. Burri, Solid State Commun. 87 (1993) 847–850.
[24] Y. Lei, L.D. Zhang, G.W. Meng, G.H. Li, X.Y. Zhang, C.H. Liang, W. Chen, S.X. Wang, Appl. Phys. Lett. 78 (2001) 1125–1127.
[25] N. Serpone, D. Lawless, R. Khairutdinov, J. Phys. Chem. 99 (1995) 16646–16654.
[26] L.V. Saraf, S.I. Patil, S.B. Ogale, S.R. Sainkar, S.T. Kshirsager, Int. J. Mod. Phys. B 12 (1998) 2635–2647.
[27] L. Forss, M. Schubnell, Appl. Phys. B 56 (1993) 363–366.
[28] D.C. Cronemeyer, Phys. Rev. 113 (1959) 1222.
[29] F. Montoncello, M.C. Carotta, B. Cavicchi, M. Ferroni, A. Giberti, V. Guidi, C. Malagu, G. Martinelli, F. Meinardi, J. Appl. Phys. 94 (2003) 1501–1505.
[30] A. Amtout, R. Leonelli, Phys. Rev. B 51 (1995) 6842.
[31] Q. Wang, J.-E. Moser, M. Grätzel, J. Phys. Chem. B 109 (2005) 14945–14953.
[32] J. Bisquert, J. Phys. Chem. B 106 (2001) 325–333.
[33] G. Kron, U. Rau, J.H. Werner, J. Phys. Chem. B 107 (2003) 13258–13261.
[34] A. Zaban, M. Greenshtein, J. Bisquert, ChemPhysChem 4 (2003) 859.
[35] P.S. Archana, R. Jose, C. Vijila, S. Ramakrishna, J. Phys. Chem. C 113 (2009) 21538–21542.
[36] J. Halme, P. Vahermaa, K. Miettunen, P. Lund, Adv. Mater. 22 (2010) E210–E234.

A list of abbreviations

BOVs: bulk oxygen vacancies
SOVs: surface oxygen vacancies
STE: self-trapped exciton
OVs: oxygen vacancies
PL: photoluminescence
DSCs: dye-sensitized solar cells
EIS: electrochemical impedance spectroscopy
OCVD: open-circuit voltage-decay
TEOA: tri-ethanolamine
ES: electrospinning
SC: spin-coating
ES-8.5: film prepared by electrospinning with 8.5 wt.% TEOA
SC-8.5: film prepared by spin-coating with 8.5 wt.% TEOA
ES-3 μm: 3 μm thick ES-8.5 film
SC-3 μm: 3 μm thick SC-8.5 film
ES-3 μm + P25: a double-layer film of ~7 μm thick P25 film on top of the ~3 μm ES-8.5 film
P25: 10 μm thick doctor-bladed P25 film